Journal of Advanced Ceramics
2018, **7**(1): 64–71
https://doi.org/10.1007/s40145-017-0257-x

ISSN 2226-4108
CN 10-1154/TQ

Research Article

Fabrication and microstructure of ZrB_2–ZrC–SiC coatings on C/C composites by reactive melt infiltration using $ZrSi_2$ alloy

Chaoqiang XUE[a,b,c], Haijun ZHOU[b,c], Jianbao HU[b,c], Hongda WANG[b,c], Jiayue XU[a], Shaoming DONG[b,c,*]

[a]*School of Materials Science and Engineering, Shanghai Institute of Technology, Shanghai 200235, China*
[b]*Structural Ceramics and Composites Engineering Research Center, Shanghai Institute of Ceramics, Chinese Academy of Sciences, Shanghai 200050, China*
[c]*State Key Laboratory of High Performance Ceramics and Superfine Microstructure, Shanghai Institute of Ceramics, Chinese Academy of Sciences, Shanghai 200050, China*

Received: September 02, 2017; Revised: December 18, 2017; Accepted: December 25, 2017

Abstract: ZrB_2–ZrC–SiC ternary coatings on C/C composites are investigated by reactive melt infiltration of $ZrSi_2$ alloy into pre-coatings. Two different pre-coating structures, including porous B_4C–C and dense C/B, are designed by slurry dip and chemical vapor deposition (CVD) process respectively. The coating prepared by reactive melt infiltration (RMI) into B_4C–C presents a flat and smooth surface with a three-layer cross-sectional structure, namely interior SiC transition layer, gradient ZrB_2–ZrC–SiC layer, and ZrB_2–ZrC exterior layer. In comparison, the coating prepared by RMI into C/B shows a more granular surface with a different three-layer cross-sectional structure, interior unreacted B–C pre-coating layer, middle SiC layer, and exterior ZrB_2–ZrC–$ZrSi_2$ layer. The forming mechanisms of the specific microstructures in two coatings are also investigated and discussed in detail.

Keywords: ultra-high temperature ceramics (UHTCs); coating; reactive melt infiltration (RMI); alloy

1 Introduction

Carbon fiber reinforced carbon matrix (C/C) composites with many merits, like low density, high retention rate of high temperature strength under inert environment, low coefficient of thermal expansion, and so on, are well regarded as one of the most promising thermal structure materials applied in aerospace fields such as nose cones and leading edges of the aircrafts [1], whereas the poor oxidation resistance of the C/C composites at temperature above 773 K seriously inhibits the further application in high temperature oxidizing atmosphere [2]. Surface coating and matrix modification are two main solutions to reduce oxygen attack level of C/C composites [3,4]. Since surface coating is already a matured technology, it is widely used in nowadays to improve the oxidation resistance properties of C/C composites.

Ultra-high temperature ceramics (UHTCs) have been increasingly developed in the past several decades in various components of reentry vehicles. It is reported that the SiC-based UHTCs, such as binary systems ZrB_2–SiC and ZrC–SiC ceramics can produce ZrO_2 and SiO_2, and form $ZrSiO_4$ by the reaction of

* Corresponding author.
E-mail: smdong@mail.sic.ac.cn

ZrO_2 and SiO_2 in the high temperature oxidizing atmosphere, which is considered as oxygen diffusion inhibition layer. Moreover, $ZrSiO_4$ not only has low permeability for oxygen and high thermal stability at high temperature, but also can reduce the consumption of SiO_2 and to a large extent improve the oxidation resistance ability of ceramics [5–7]. Owing to these advantages, introducing UHTCs into coating is considered to be a promising solution to the poor oxidation resistance of C/C composites. Up to now, a large number of efforts have been made to fabricate UHTCs–SiC coatings, and some key methods have been adopted like reactive melt infiltration (RMI), pack cementation, and supersonic plasma spraying (SPS), etc. [8–14]. Zhang *et al.* [15] selected supersonic atmosphere plasma spraying (SAPS) with ZrB_2–SiC–ZrC as raw materials to form ZrB_2–SiC–ZrC coating by the high temperature of a plasma arc and the high velocity of particles. Qi *et al.* [16] prepared ZrB_2–SiC/SiC coating on C_f/SiC composites at 1900 ℃ by pack cementation. Compared to SPS and pack cementation, RMI can avoid the oxidation during the fabrication, needs lower temperature with alloy, and can form a dense structure. It is well known that preparation of porous structure is critical to the RMI for a dense structure and better oxidation/ablation resistance properties [17–22]. As we know, slurry dip with resin phenolic as material is usually used to introduce carbon to the composites, and it can produce porous structure after pyrolysis.

In this work, a ZrB_2–ZrC–SiC ternary system coating is prepared on C/C composites by RMI using $ZrSi_2$ alloy based on slurry dip prepared B_4C/C pre-coating. A porous B_4C/C pre-coating is prepared by slurry dip and pyrolysis with resin phenolic as raw material and then the molten $ZrSi_2$ alloy is infiltrated into the porous pre-coating and finally ZrB_2–ZrC–SiC coating is obtained after in-situ reaction between B_4C/C and $ZrSi_2$. For a comparison, a boron and carbon containing pre-coating prepared by chemical vapor deposition (CVD) is applied as well. The microstructure and formation mechanisms of the ZrB_2–ZrC–SiC coatings are studied and discussed in detail.

2 Experimental procedures

2. 1 Pre-coating preparation

B_4C/C pre-coating and boron and carbon containing pre-coating were prepared by slurry dip and CVD respectively in this paper. For B_4C/C pre-coating, B_4C powder (98.5% purity, Mudanjiang Abrasive and Grinding Tools, China) and phenolic resin (Shanghai Qinan Adhesive Material Factory, China) were mixed in alcohol through ball milling to obtain a slurry. Substrates (40 mm × 6 mm × 3.5 mm) were machined from 2D C/C composites which were fabricated through polymer infiltration and pyrolysis (PIP). Its density and open porosity are 1.6 g/cm^3 and 9% respectively measured by Archimedes method with deionized water as medium. Then, substrates were dipped in the above-mentioned slurry and dried in air. After that, the slurry dip coating was cured at 120–150 ℃ for 1 h. The above processes were repeated for several times to obtain an expected thickness for pre-coating. Ultimately, the pre-coating was heated at 1500 ℃ before RMI for sake of transferring B_4C/resin into B_4C/C pre-coating. For boron and carbon containing pre-coating, BCl_3 and C_2H_4 gases were selected as the sources of B and C respectively, H_2 as the catalyst, and Ar as the carrier gas. Procedures like putting the C/C substrates in CVD device, controlling calculated flux of those mixed gases by flow controller, heating the device with the rate of 5 ℃/min to 1000 ℃ and maintaining 14 h were carried out to obtain boron and carbon containing pre-coating.

2. 2 Coating preparation

C/C composites coated with B_4C/C or boron and carbon containing pre-coating were placed in a graphite crucible containing some $ZrSi_2$ alloy at the bottom. Then the furnace was heated to 1800 ℃ and dwelled for 2 h in vacuum. During the process, the molten $ZrSi_2$ penetrated into the pre-coating and reacted with carbon, B_4C, or boron and carbon containing phase to form ZrB_2–ZrC–SiC coating.

2. 3 Microstructure analysis

The composition variation of the coating was analyzed by X-ray diffraction (Model D/max 2550 V, Rigaku, Japan) with Cu Kα source. The microstructure was observed by a S4800 field emission scanning electron microscope (Hitachi, Tokyo, Japan) equipped with energy-dispersive spectroscopy (EDS, Inca Energy) for elemental analysis. The densities and open porosities of substrates were measured by Archimedes method with deionized water.

3 Results and discussion

3. 1 Pre-coating

Figure 1 shows the SEM images of cross-sections and surfaces of slurry dip prepared B_4C/C pre-coating after heat treatment at 1500 ℃ and CVD prepared boron and carbon containing pre-coating. It can be observed that both pre-coatings are continuous and integral. As shown in Fig. 1(a), the slurry dip pre-coating is well connected with substrate without obvious cracks and the thickness of the pre-coating is about 130 μm. Due to the volume shrinkage and emission of gas products during the resin organic compound pyrolysis at high temperature, this pre-coating structure is loose and quite a few pores could be observed. In addition, it is clear that B_4C particles are surrounded by pyrolysis carbon and many pores can be discovered in Fig. 1(b). It is well known that the porous structure has a positive effect on the densification during RMI process, which is helpful to obtain a dense structure.

In Figs. 1(c) and 1(d), the CVD prepared pre-coating is also well connected with the substrate without any cracks. But unlike the slurry dip pre-coating, the CVD prepared pre-coating structure is exceedingly compact. In addition, the CVD prepared pre-coating surface morphology shows a micro-scale nodular structure, which is in accordance with results presented in literatures [23–25].

Figure 2 represents the XRD patterns of both pre-coatings. Clearly, B_4C and carbon diffraction peeks could be found in slurry dip pre-coating in Fig. 2(a). Although only low crystalline pyrolytic carbon (PyC) diffraction peak is detected on the XRD pattern of the CVD pre-coating, both boron and carbon elements are detected by EDS in Fig. 1(c). It can be concluded that the CVD pre-coating is primarily composed of carbon and boron phases.

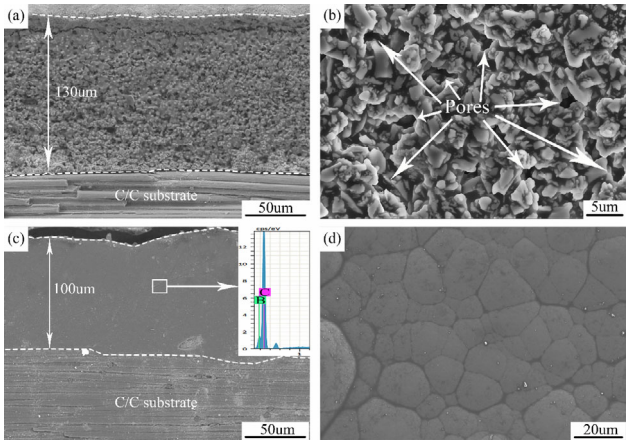

Fig. 1 Cross-section and surface microstructure of (a, b) slurry dip pre-coating and (c, d) CVD pre-coating.

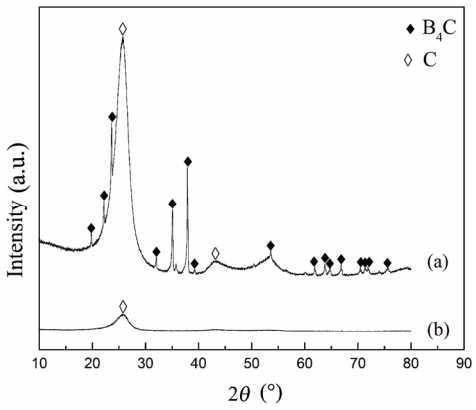

Fig. 2 XRD patterns of (a) slurry dip pre-coating and (b) CVD pre-coating.

3. 2 ZrB_2–ZrC–SiC coating

During RMI process, the molten $ZrSi_2$ would infiltrate into the pre-coating by capillary force and react with pre-coating. Figure 3 shows morphology of the RMI prepared coating based on slurry dip pre-coating. As shown in Fig. 3(a), the coating surface is flat and smooth without any apparent defects like large cracks or bumps, which would reduce the passage for oxygen going through the substrate and decrease the heat flow scouring. The XRD results of the surface in Fig. 4(a) indicate that the diffraction peaks of ZrB_2 and ZrC phases are detected, while SiC phase cannot be observed. From Figs. 3(b) and 3(c), it could be observed that the molten $ZrSi_2$ alloy reacts with B_4C/C pre-coating completely and the thickness of the coating increases from 130 to ~180 μm. The increment of its thickness is attributed to the volume expansion by reactions. The molar volumes of B_4C, ZrC, and ZrB_2 are 21.93, 15.34, and 18.54 cm^3/mol, respectively. Therefore, when B_4C reacts with Zr to form ZrC and ZrB_2, the volume expands by 139%. Besides, it is generally believed that the similar volume expansion occurs during the reaction between carbon and Zr–Si eutectic.

In addition, there are only white and gray phases in cross-section backscattered images of the coating in Fig. 3(b). From EDS analysis (Spot1, Spot2, Spot3) in Fig. 3 and XRD pattern result of coating surface in Fig. 4(a), it could be revealed that the white phase is mixed phase of ZrC and ZrB_2 and the gray phase is SiC.

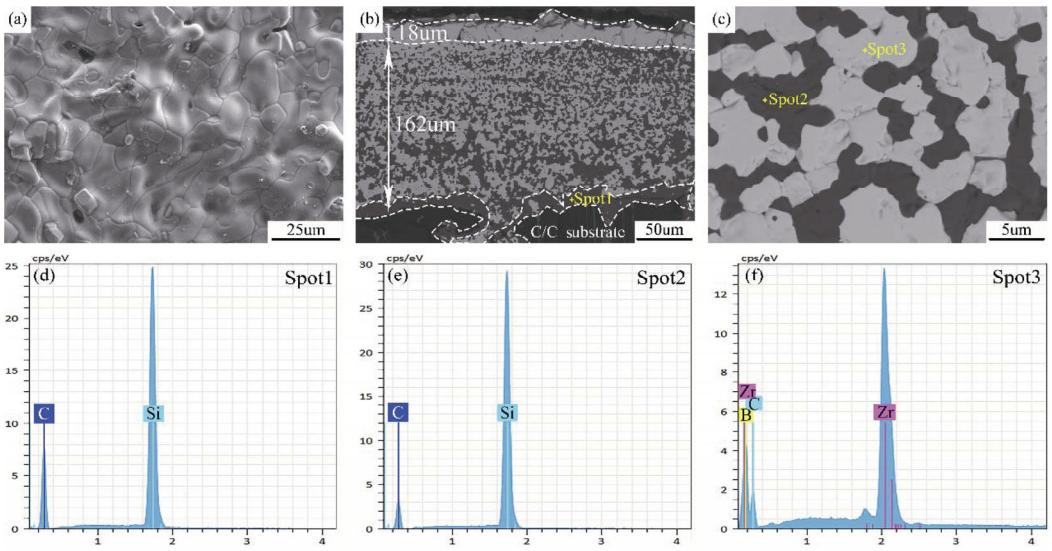

Fig. 3 Microstructure of ZrB_2–ZrC–SiC coating based on slurry dip pre-coating: (a) surface, (b) cross-section, (c) high magnification of cross-section. (d)–(f) EDS analysis of different spots.

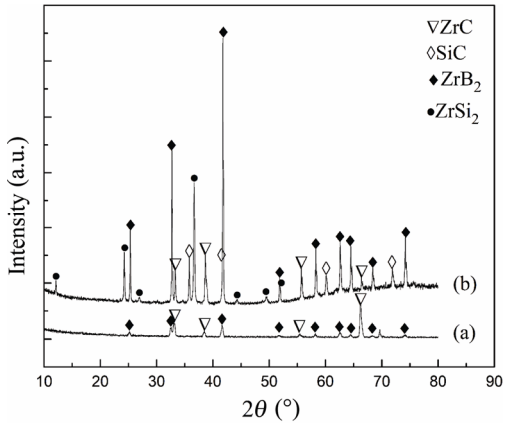

Fig. 4 XRD patterns of ZrB_2–ZrC–SiC coating based on (a) slurry dip pre-coating and (b) CVD pre-coating.

Interestingly, it can also be observed that the coating is comprised of three layers with different constituent distribution. The exterior layer is a white phase with a thickness of about 18 μm, which could explain the absence of SiC phase in the XRD pattern result. The middle layer is composed of white phase and gray phase, which are both distributed in a slight gradient trend. The interior layer is SiC, which is known as reaction bonding layer. It can finely enhance the boning strength between substrate and the coating and has a positive effect on declining the mismatch of coefficient of thermal expansion (CTE) between them.

Figure 5 shows the microstructure of ZrB_2–ZrC–SiC coating obtained from CVD pre-coating. In Fig. 5(a), it can be found that the surface of coating is also smooth but more granular compared to the coating based on slurry dip pre-coating, and the salient tetragonal grain morphology belongs to ZrB_2. Besides ZrB_2, ZrC, and SiC, $ZrSi_2$ phases are also detected by the XRD pattern of coating surface in Fig. 4(b). Similar to the coating based on slurry dip pre-coating, this coating is also divided into three layers namely exterior white layer, middle gray layer, and interior unreacted dark layer.

As marked in Fig. 5(b), the exterior and middle layers are only about 33 μm in total and the interior unreacted layer is amounted to 77 μm, which suggests only a small part of CVD pre-coating reacts with $ZrSi_2$. From the high magnification backscattered cross-section image of the coating in Fig. 5(c), it could be discovered that the exterior white layer is composed of two phases, distinguished by their slightly different contrasts. Through the EDS (Spot2, Spot3) in Fig. 5, and the XRD pattern result in Fig. 4(b), it could be inferred that in the exterior white layer, the darker part is $ZrSi_2$ and the whiter part is composed of ZrB_2 and ZrC. There is also a little SiC observed in the exterior layer, which results in the existence of SiC phase in the XRD pattern of the coating surface. As for the middle gray layer, it should be SiC phase, as detected by EDS (Spot1) in Fig. 5.

3. 3 Coating formation mechanism

From the Zr–Si phase diagram [26], it can be known that the melting point of $ZrSi_2$ alloy is 1620 ℃ and at this temperature the alloy is consisted of solid β-ZrSi phase and liquid Zr–Si eutectic. As temperature increases, more β-ZrSi will transfer to Zr–Si eutectic according to lever principle. Therefore, when the

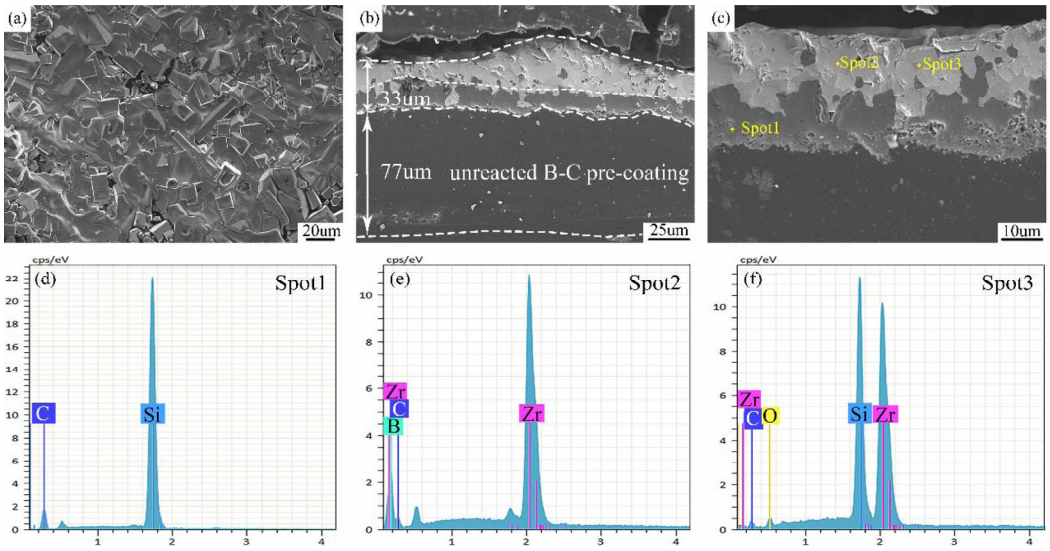

Fig. 5 Microstructure of ZrB_2–ZrC–SiC coating based on CVD pre-coating: (a) surface, (b) cross-section, (c) high magnification of cross-section. (d)–(f) EDS analysis of different spots.

temperature is raised up to 1800 ℃, Zr–Si eutectic will account for a large proportion and react with pre-coating. All the reactions involved in the whole process are given as below:

$$Si + C = SiC \quad (1)$$

$$Zr + C = ZrC \quad (2)$$

$$B_4C + Zr = ZrC + 2ZrB_2 \quad (3)$$

$$SiC + Zr = ZrC + Si \quad (4)$$

Changes in Gibbs free energy of reactions as a function of temperature are shown in Fig. 6. The Gibbs free energies of reactions from reactions (1) to (4) at 1800 ℃ are −10.36, −41.93, −162.21, and −31.57 $kJ \cdot mol^{-1}$, respectively. The negative Gibbs free energy demonstrates that all the reactions are favorable thermodynamically. Besides, the more negative Gibbs free energy of reactions (2), (3), and (4) than that of reaction (1) indicates that Zr element is more active than Si element during the reactions.

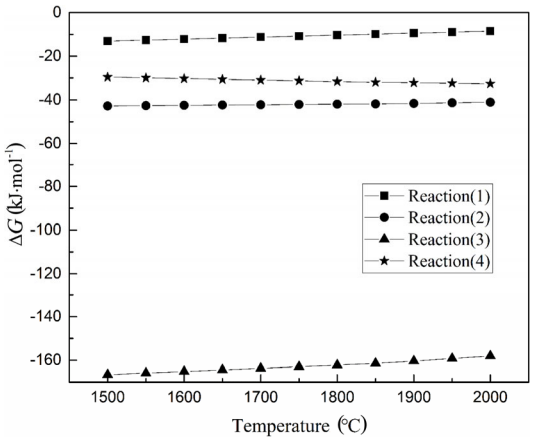

Fig. 6 Changes in Gibbs free energy of reactions with temperature.

The schematic diagram of ZrB_2–ZrC–SiC coating based on slurry dip pre-coating during the RMI process is presented in Fig. 7. In step (a), owning to the porous and loose structure of slurry dip pre-coating, molten Zr–Si eutectic will infiltrate into the pores by the capillary force. In step (b), the constantly proceeding Zr–Si eutectic through the pores would simultaneously react with B_4C/C to form ZrB_2/ZrC and SiC by above reactions, which also makes the pores smaller due to the volume expansion. In step (c), as the infiltration and reaction continue, Zr–Si eutectic goes deeper and more B_4C/C is transformed into ZrB_2/ZrC and SiC. As mentioned above, Zr is more active than Si, which means that the consumption rate of Zr is faster than Si during the infiltration. Moreover, the amount of Si is more than Zr in the eutectic originally. Therefore, it is unavoidable that the proportion of Zr becomes less compared to Si in Zr–Si eutectic as the infiltration continues. Finally, it leads to the slightly gradient distribution of SiC and ZrB_2/ZrC along coating direction. It is worth noting that the replacement reaction between Zr and SiC according to reaction (4) is favorable when the quantity of Zr is adequate at the beginning of infiltration but impractical as the infiltration goes deep, leading to fewer SiC in the exterior layer. In step (d), near the end of the infiltration, the most outer pores are fully filled by ZrB_2/ZrC and SiC, leaving a small inner part still containing some Zr–Si eutectic which is dominated by

Si with few Zr. In step (e), the remained Zr–Si eutectic would finally contact with surface of C/C composites to form a reaction bonding SiC layer between the C/C composites and exterior coating.

The formation mechanism of ZrB_2–ZrC–SiC coating from CVD pre-coating is shown in Fig. 8. In step (a), unlike slurry dip pre-coating, CVD pre-coating has a compact and dense structure, where the molten Zr–Si eutectic could not directly infiltrate into the pre-coating by capillary force. It has been reported that the formation of ceramic–metal composites was proposed by following: heating the reactive metal particulates to be molten, then molten metal wetting the ceramic and reacting with boron carbide [27]. Thus, in CVD–RMI process, it can be deduced that when the $ZrSi_2$ alloy melts and contacts with the pre-coating, it would wet the pre-coating by the surface tension (γ_{SV}, γ_{LV}, γ_{SL}). Zr–Si eutectic will gradually spread and finally cover

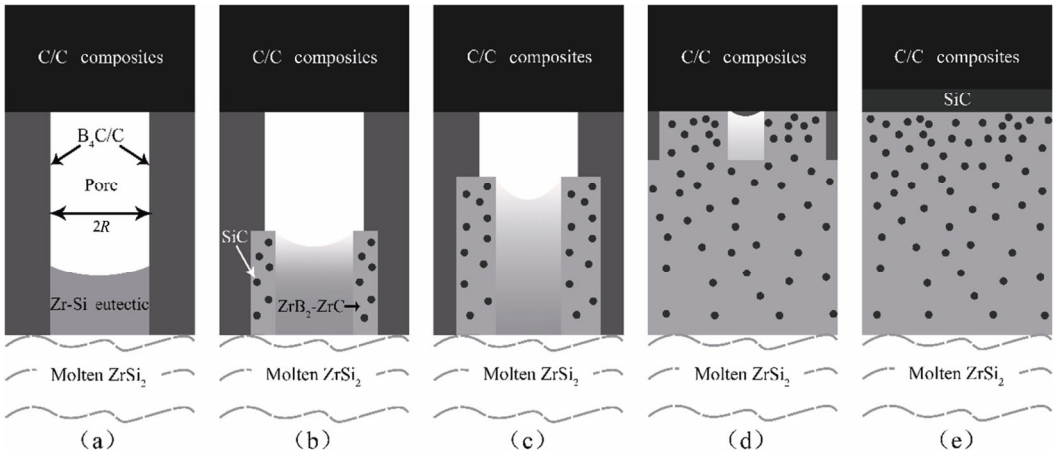

Fig. 7 Schematic diagram of ZrB_2–ZrC–SiC coating based on slurry dip pre-coating.

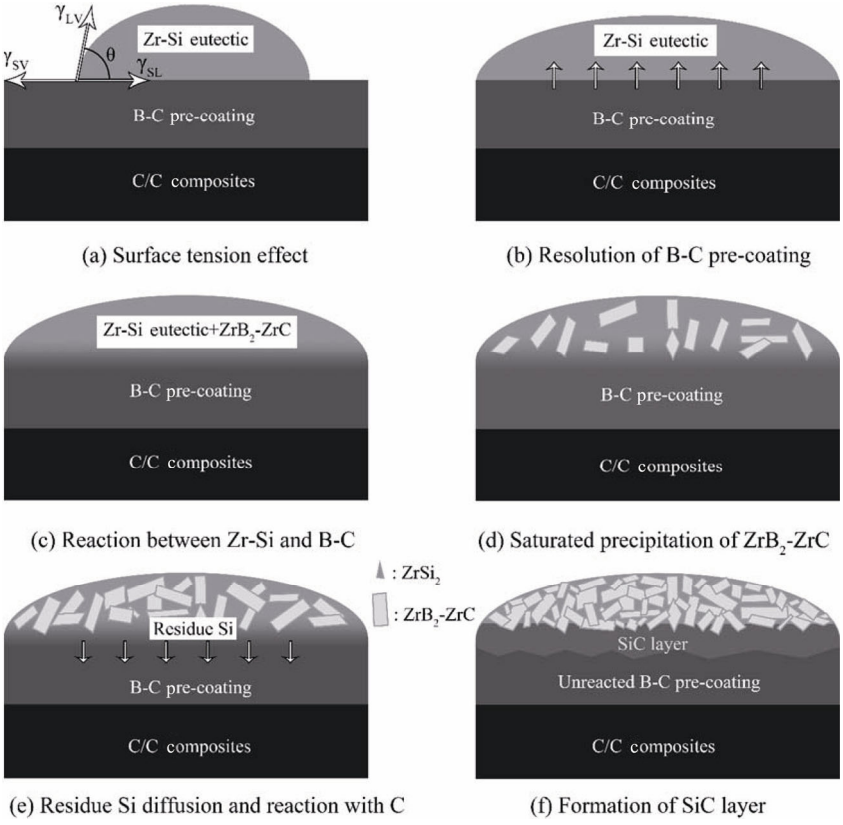

Fig. 8 Schematic diagram of ZrB_2–ZrC–SiC coating based on CVD pre-coating.

the surface of the coating. In steps (b) and (c), boron carbon compound dissolves in the molten Zr–Si eutectic owning to the heat of eutectic, and in the meantime boron–carbon compound preferentially reacts with Zr to form ZrB_2/ZrC by reactions (2) and (3) due to their more negative Gibbs energy. Although carbon can partially react with Si by reaction (1), a replacement reaction between Zr and SiC might happen according to reaction (4) whose Gibbs free energy is more negative than that of reaction (1). So, at this stage the melt mainly consists of Zr–Si eutectic, ZrB_2, and ZrC. In step (d), as the dissolution and reaction continue, more ZrB_2 and ZrC is formed in the melt and ultimately precipitates when the melt saturates. In step (e), the saturation–precipitation process will be faster when the temperature goes down. And when temperature is relatively low, remained Si with low melt point still has low viscosity which enables it to flow through the gap of ZrB_2 and ZrC, and reacts with the dissolved carbon to form a thin SiC layer. Some $ZrSi_2$ phases are also formed by the reaction between residue Zr and Si, which is surrounded by ZrB_2–ZrC in exterior layer when the temperature goes down. Unfortunately, a large amount of unreacted carbon boron compound from the pre-coating still exists at the end, which might be attributed to the formation of ZrB_2–ZrC diffusion barrier and the limited thickness of the covered Zr–Si eutectic on the surface of pre-coating.

4 Conclusions

In this work, ZrB_2–ZrC–SiC coatings were successfully prepared by RMI of $ZrSi_2$ alloy into porous B_4C–C or C/B pre-coatings, where the pre-coatings were fabricated by slurry dip and CVD. Slurry dip prepared pre-coating has a porous and loose structure which is beneficial for deep infiltration of Zr–Si eutectic. The formation of ZrB_2–ZrC–SiC coating based on porous B_4C–C pre-coating is mainly by capillary force and reactions among Zr–Si eutectic, B_4C, and C. The as-prepared ZrB_2–ZrC–SiC coating possesses a flat and smooth surface morphology and three-layer cross structure namely SiC interior transition layer, gradient ZrB_2–ZrC–SiC middle layer, and ZrB_2–ZrC exterior layer. The thickness of the coating expanded from 130 to 180 μm. While CVD prepared pre-coating has an extremely compact and dense structure which severely inhibits the infiltration of Zr–Si eutectic. Consequently, the formation mechanism of ZrB_2–ZrC–SiC coating based on CVD prepared C/B pre-coating is mainly via the spread of Zr–Si eutectic by surface extension effect on the coating surface and reactions between dissolved pre-coating and Zr–Si eutectic. CVD combined RMI prepared coating presents a smooth but more granular surface morphology than the former and has three-layer cross structure namely interior unreacted C/B pre- coating layer, SiC middle layer, and ZrB_2–ZrC–$ZrSi_2$ exterior layer. The thickness of the coating expanded from 100 to ~110 μm.

Acknowledgements

The authors are grateful to the financial support from the National Key Research and Development Program of China (No. 2017YFB0703200), and the research grant from Science and Technology Commission of Shanghai Municipality (No. 16DZ2260600).

References

[1] Savage G. *Carbon–Carbon Composites*. London: Chapman & Hall, 1993.

[2] Dhami TL, Bahl OP, Awasthy BR. Oxidation-resistant carbon–carbon composites up to 1700 ℃. *Carbon* 1995, **33**: 479–490.

[3] Joshi A, Lee JS. Coatings with particulate dispersions for high temperature oxidation protection of carbon and C/C composites. *Composites Part A* 1997, **28**: 181–189.

[4] Alvey MD, George PM. $ZrPt_3$ as a high-temperature, reflective, oxidation-resistant coating for carbon–carbon composites. *Carbon* 1991, **29**: 523–530.

[5] Zhou H-J, Feng Q, Kan Y-M, *et al*. ZrB_2–SiC coatings prepared by vapor and liquid silicon infiltration methods: Microstructure and oxidation resistance property. *J Inorg Mater* 2013, **28**: 1158–1162. (in Chinese)

[6] Rezaie A, Fahrenholtz WG, Hilmas GE. The effect of a graphite addition on oxidation of ZrB_2–SiC in air at 1500 ℃. *J Eur Ceram Soc* 2013, **33**: 413–421.

[7] Williams PA, Sakidja R, Perepezko JH, *et al*. Oxidation of ZrB_2–SiC ultra-high temperature composites over a wide range of SiC content. *J Eur Ceram Soc* 2012, **32**: 3875–3883.

[8] Einset EO. Analysis of reactive melt infiltration in the processing of ceramics and ceramic composites. *Chem Eng Sci* 1998, **53**: 1027–1039.

[9] Chen X, Dong S, Kan Y, *et al*. 3D C_f/SiC–ZrC–ZrB_2 composites fabricated via sol–gel process combined with reactive melt infiltration. *J Eur Ceram Soc* 2016, **36**: 3607–3613.

[10] Pi H, Fan S, Wang Y. C/SiC–ZrB_2–ZrC composites fabricated by reactive melt infiltration with $ZrSi_2$ alloy. *Ceram Int* 2012, **38**: 6541–6548.

[11] Hu C, Niu Y, Huang S, *et al*. In-situ fabrication of ZrB_2–SiC/SiC gradient coating on C/C composites. *J Alloys Compd* 2015, **646**: 916–923.

[12] Jia Y, Li H, Li L, *et al*. Effect of monolithic LaB_6 on the ablation resistance of ZrC/SiC coating prepared by supersonic plasma spraying for C/C composites. *J Mater Sci Technol* 2016, **32**: 996–1002.

[13] Abdollahi A, Ehsani N, Valefi Z. Thermal shock resistance and isothermal oxidation behavior of C/SiC–SiC_{nano} functionally gradient coating on graphite produced via reactive melt infiltration (RMI). *Mater Chem Phys* 2016, **182**: 49–61.

[14] Zhou H, Gao L, Wang Z, *et al*. ZrB_2–SiC oxidation protective coating on C/C composites prepared by vapor silicon infiltration process. *J Am Ceram Soc* 2010, **93**: 915–919.

[15] Zhang Y, Hu H, Zhang P, *et al*. SiC/ZrB_2–SiC–ZrC multilayer coating for carbon/carbon composites against ablation. *Surf Coat Technol* 2016, **300**: 1–9.

[16] Qi Y-S, Wang Y-Y, Zhou C-L, *et al*. On the ZrB_2–SiC/SiC ultrahigh temperature ceramics coating for C_f/SiC composition. *Adv Ceram* 2016, **37**: 119–125. (in Chinese)

[17] Zou L, Wali N, Yang J-M, *et al*. Microstructural development of a C_f/ZrC composite manufactured by reactive melt infiltration. *J Eur Ceram Soc* 2010, **30**: 1527–1535.

[18] Hillig WB. Melt infiltration approach to ceramic matrix composites. *J Am Ceram Soc* 1988, **71**: C-96–C-99.

[19] Zhu Y, Wang S, Li W, *et al*. Preparation of carbon fiber-reinforced zirconium carbide matrix composites by reactive melt infiltration at relative low temperature. *Scripta Mater* 2012, **67**: 822–825.

[20] Chen X, Dong S, Kan Y, *et al*. 3D C_f/SiC–ZrC–ZrB_2 composites fabricated via sol–gel process combined with reactive melt infiltration. *J Eur Ceram Soc* 2016, **36**: 3607–3613.

[21] Li Z, Li H, Zhang S, *et al.* Microstructure and ablation behaviors of integer felt reinforced C/C–SiC–ZrC composites prepared by a two-step method. *Ceram Int* 2012, **38**: 3419–3425.

[22] Pi H, Fan S, Wang Y. C/SiC–ZrB_2–ZrC composites fabricated by reactive melt infiltration with $ZrSi_2$ alloy. *Ceram Int* 2012, **38**: 6541–6548.

[23] Zeng B, Feng Z, Li S, *et al*. Microstructure and deposition mechanism of CVD amorphous boron carbide coatings deposited on SiC substrates at low temperature. *Ceram Int* 2009, **35**: 1877–1882.

[24] Li S, Zeng B, Feng Z, *et al*. Effects of heat treatment on the microstructure of amorphous boron carbide coating deposited on graphite substrates by chemical vapor deposition. *Thin Solid Films* 2010, **519**: 251–258.

[25] Berjonneau J, Chollon G, Langlais F. Deposition process of amorphous boron carbide from CH_4/BCl_3/H_2 precursor. *J Electrochem Soc* 2006, **153**: C795–C800.

[26] Tong Y, Bai S, Chen K. C/C–ZrC composite prepared by chemical vapor infiltration combined with alloyed reactive melt infiltration. *Ceram Int* 2012, **38**: 5723–5730.

[27] Halverson DC, Pyzik AJ, Aksay IA. Boron–carbide–aluminum and boron–carbide–reactive metal cermets. U.S. Patent 4,605,440. 1986.